JOURNAL OF SOLID STATE CHEMISTRY 62, 64–74 (1986)

Hydrothermal Synthesis and Structure of $Cu_6^{1+}Mo_5^{6+}O_{18}$

E. M. McCARRON III AND J. C. CALABRESE

Central Research and Development Department, E. I. duPont de Nemours and Company Experimental Station, Wilmington, Delaware 19898

Received March 4, 1985; in revised form July 29, 1985

Single crystals of $Cu_6^{1+}Mo_5^{6+}O_{18}$ have been grown both hydrothermally and by the Bridgman technique from stoichiometric mixtures of the binary oxides. $Cu_6Mo_5O_{18}$ crystallizes in the space group $I2/c$ with cell parameters $a = 14.702$, $b = 6.272$, $c = 15.264$ Å, $\beta = 101.87°$, $V = 1377.46$ Å^3, and $Z = 4$. The structure was solved by the Patterson method and refined to $R = 0.027$ using 1164 independent reflections. The structure can be described as chains of edge-sharing MoO_6 octahedra running along the a axis between sheets (ab plane) of corner-sharing CuO_4 tetrahedra. Within the molybdenum chains there are three independent molybdenum atoms, each exhibiting a different type of distortion from octahedral site symmetry. Short Cu–Cu contacts (<2.8 Å), similar to Cu^{1+} aggregate compounds, are found within the Cu layers. The relationship of $Cu_6Mo_5O_{18}$ to the thermal reduction of $Cu_3Mo_2O_9$ is discussed.

1. Introduction

Solid state synthesis in the CuO–MoO_3 system is complicated by an accompanying loss of oxygen at temperatures only slightly higher than the melting points of mixtures of the simple oxides (*1*). This shift from cupric to cuprous compound formation has been held responsible for a number of inconsistencies and controversies concerning the exact nature of the Cu_2O–CuO–MoO_3 phase diagram (*1–6*).

One such case involves the thermal reduction of $Cu_3Mo_2O_9$. Thomas *et al.* (*7*) reported the so-called "breathing" mode for the reaction

$$Cu_3Mo_2O_9 \rightleftarrows Cu_3Mo_2O_8 + \tfrac{1}{2}O_2. \quad (1)$$

In a more detailed study, Nassau and Shiever (*1*) reported a weight loss of 4.6% for $Cu_3Mo_2O_9$ implying the formation of $Cu_6Mo_4O_{15}$:

$$2Cu_3Mo_2O_9 \rightarrow Cu_6Mo_4O_{15} + \tfrac{3}{2}O_2. \quad (2)$$

Subsequently, Kihlborg (*8, 9*) and co-workers addressed this problem crystallographically, solving the structures of both $Cu_3Mo_2O_9$ and $Cu_{4-x}Mo_3O_{12}$. $Cu_{4-x}Mo_3O_{12}$ was shown to have a unit cell identical with that reported for $Cu_3Mo_2O_8$ by Thomas *et al.* (*7*), implying that the latter composition was in error. Kihlborg did not observe any simple structural relationship between $Cu_3Mo_2O_9$ and $Cu_{4-x}Mo_3O_{12}$. Moreover, the change in the Cu/Mo ratio upon reduction implies that the reduction mechanism is complex, requiring the formation of at least two copper-containing phases:

$$3Cu_3Mo_2O_9 \rightarrow 2Cu_{4-x}Mo_3O_{12} + (\tfrac{1}{2} + x)Cu_2O + ((5 - 2x)/4)O_2. \quad (3)$$

0022-4596/86 $3.00

In more recent studies, Machej and Ziolkowski (*2, 3*) reported that during the initial stages of reduction of $Cu_3Mo_2O_9$, $Cu_{4-x}Mo_3O_{12}$ is indeed produced, but that upon further reduction, $Cu_6Mo_4O_{15}$ is formed in accord with the results of Nassau and Shiever (*1*). This observation implies that the Cu_2O formed in the initial stages of reduction (Eq. (3)) is reincorporated into the molybdate phase to form $Cu_6Mo_4O_{15}$. Machej and Ziolkowski (*2*) thus claimed to have finally settled this long-standing controversy. They further reported that $Cu_6Mo_4O_{15}$ exhibits a temperature-independent paramagnetism. This paramagnetism is at odds with the formulation, $Cu_6^{1+}Mo_4^{6+}O_{15}$, suggesting the presence of an impurity phase.

In this paper, we report the formation and structure of $Cu_6Mo_5O_{18}$ which is apparently the pure phase erroneously reported as $Cu_6Mo_4O_{15}$ (*1–6, 10*). This finding confirms that there exists no simple "breathing" mechanism responsible for the interconversion between cupric and cuprous molybdates. In fact, the thermal reduction of $Cu_3Mo_2O_9$ can now be viewed as proceeding in at least two stages, each stage involving not only reduction of Cu^{2+} to Cu^{1+} but also formation of Cu_2O. The formation of Cu_2O accounts for the observed decrease in the Cu/Mo ratio of the resulting molybdate as a function of the degree of reduction:

$$Cu_3Mo_2O_9 \xrightarrow{1} Cu_{4-x}Mo_3O_{12}\ (x \sim 0.15) \xrightarrow{2} Cu_6Mo_5O_{18}. \quad (4)$$

The balanced equation for the first stage of the reduction is given by Eq. (3) above and for the second stage by the equation

$$5Cu_{4-x}Mo_3O_{12} \rightarrow 3Cu_6Mo_5O_{18} + ((2 - 5x)/2)Cu_2O + ((22 + 5x)/4)O_2. \quad (5)$$

2. Experimental

Hydrothermal synthesis. Stoichiometric quantities of cuprous oxide and molybdenum trioxide necessary to make 5-g samples of $Cu_6Mo_5O_{18}$ were weighed into gold tubes, $\frac{3}{8}$ in. in diameter and 6 in. long. Five milliliters of water was added to each tube and the tubes were then sealed in air. Filled tubes were subjected to 3 kilobars of pressure. This pressure was maintained while the tubes were heated to 500°C for 12 hr and subsequently slow cooled (10°C/hr) to room temperature. When opened, the tubes were observed to contain beautifully faceted, dark metallic-looking crystals of millimeter dimensions. The crystals were water-washed and air-dried. A streak test revealed that the crystals were actually red colored. Very thin crystals were observed under the microscope to transmit red light. A crystal grown in the above described manner was selected for the structure determination.

Bridgman growth. For measurement of the electrical properties larger crystals than those grown hydrothermally were desired. Since $Cu_6Mo_5O_{18}$ was observed to melt congruently (see Fig. 1), the standard Bridgman technique (*11*) was applied. Boules 1 cm in diameter were produced from which crystals of several millimeters on an edge could be cleaved.

Electrical measurements. Resistivity measurements were made on single crystals of $Cu_6Mo_5O_{18}$ utilizing a standard 4-probe technique. Indium contacts were soldered onto the crystals in a nitrogen atmosphere to avoid oxidation.

Analysis. The chemical composition of single crystals of $Cu_6Mo_5O_{18}$ was checked by both conventional chemical and electron microprobe analysis. The results were as follows: standard chemical analysis (*12*)—Cu = 31.7(3)%, Mo = 40.3(4)%, and O = 27.6(3)%; microprobe analysis—Cu = 28.8(1.4%) and Mo = 41.6(2.1)%; calcu-

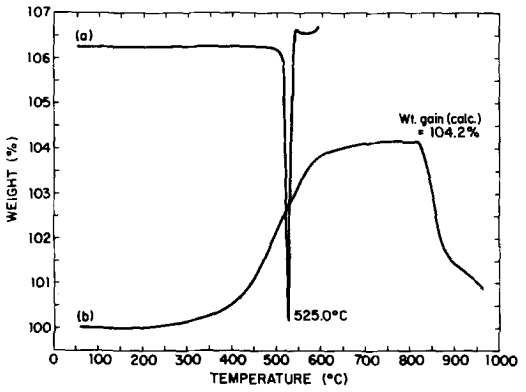

FIG. 1. (a) DSC (nitrogen) and (b) TGA (oxygen) data for $Cu_6Mo_5O_{18}$. The observed TGA weight gain of ~4.2% is in excellent agreement with the oxygen uptake calculated for $Cu^{1+} \rightarrow Cu^{2+}$.

lated for $Cu_6Mo_5O_{18}$—Cu 33.18%, Mo = 41.75%, and O = 25.07%.

Thermoanalysis. Thermogravimetric analyses were carried out on a DuPont 951-1090B instrument at a heating rate of 5°C/min in an oxygen atmosphere. Differential scanning calorimetry was performed with a DuPont 910-1090B instrument at a heating rate of 5°C/min in a nitrogen atmosphere. Both traces are displayed in Fig. 1.

X-Ray powder diffraction. X-Ray powder diffraction patterns were obtained with a Guinier-Hägg type focusing camera (r = 40 mm). The radiation was monochromatic Cu$K\alpha_1$ (λ = 1.5405 Å) and the internal standard was silicon (a = 5.4305 Å). An Optronics P-1700 photomation instrument was used to collect absorbance data from the films. Peak positions and relative intensities were determined with local computer programs. The lattice parameters were refined by a least-squares procedure. The refined monoclinic lattice parameters for $Cu_6Mo_5O_{18}$ are a = 14.703(2), b = 6.272(1), c = 15.264(2) Å, and β = 101.87(1)°; with figures of merit M_{20} = 42 (*13*) and F_{20} = 92 (7.5 × 10^{-3}, 29) (*14*).

The X-ray powder diffraction data for $Cu_6Mo_5O_{18}$ is compared with the pattern reported for $Cu_6Mo_4O_{15}$ (*2*) in Table I. Also

TABLE I

OBSERVED AND CALCULATED POWDER PATTERNS FOR $Cu_6Mo_5O_{18}$

hkl	2θ	*d*(obs)	*d*(calc)	*I*	*I*(cal)	$Cu_6Mo_4O_{15}$(2)
002	11.837	7.469	7.46885	8	3.6	
200	12.301	7.189	7.19410	6	3.3	
011	15.305	5.784	5.78281	40	36.7	5.77 (m)
−202			5.81333		2.1	
110			5.74938		0.0	
−211	18.887	4.694	4.69342	20	12.4	4.69 (vw)
202			4.71898		1.0	
112	20.242	4.383	4.38497	11	4.9	4.38 (vw)
013	22.784	3.899	3.89970	15	9.6	3.89 (vw)
310	23.325	3.810	3.80981	13	6.0	3.80 (vw)
004	23.797	3.735	3.73443	15	8.0	3.72 (vw)
−213	24.101	3.689	3.68627	3	3.5	
−312	24.407	3.643	3.64334	66	42.9	3.63 (w)
−204			3.63428		18.3	
400	24.713	3.599	3.59705	3	2.2	
−402	25.151	3.537	3.53779	13	6.7	3.53 (vw)
−114	27.372	3.255	3.25645	11	4.8	[3.42 (vw)][a]
213	27.671	3.220	3.21804	18	15.4	
312	27.945	3.190	3.18936	100	100.0	3.18 (ms)
204	29.092	3.066	3.06652	1	1.2	
−121	29.483	3.027	3.02773	52	39.3	3.02 (w)
114	29.545	3.020	3.02040	19	15.6	
121	29.992	2.976	2.97595	64	49.6	2.974 (vs)
411	30.268	2.959	2.95079	73	58.0	2.947 (m)
−314	30.638	2.915	2.91571	95	92.5	2.913 (s)
−404	30.698	2.909	2.90666	39	34.9	
−413	30.951	2.886	2.88591	57	34.2	2.889 (m)
022			2.89141		25.1	
−222	32.425	2.758	2.75997	4	1.5	
015	33.184	2.697	2.69718	52	46.5	2.696 (ms)
−215			2.69544		0.1	
−123	33.640	2.661	2.66209	9	3.1	
−321	33.969	2.636	2.63615	17	12.8	2.630 (vw)
−512	34.078	2.628	2.62645	6	5.9	
510	34.253	2.615	2.61548	17	0.3	
222			2.61182		8.5	
321	35.357	2.536	2.53684	27	25.0	2.534 (w)
006	36.048	2.489	2.48962	21	11.8	
314	36.297	2.472	2.47253	31	23.0	
413	36.582	2.454	2.45428	28	19.5	
−602	36.907	2.433	2.43361	26	11.2	
−323			2.43782		6.4	
024	37.411	2.401	2.40151	20	10.1	
600			2.39803		7.1	
−415	37.760	2.380	2.38055	34	18.5	
215			2.38415		17.0	
−224			2.37424		3.1	
−116	38.161	2.356	2.35635	17	8.7	
404			2.35949		0.7	
−514			2.35965		1.5	
512	38.512	2.335	2.33600	14	7.5	
−316	39.880	2.258	2.26008	5	1.2	
−604	40.273	2.237	2.23800	11	4.6	
323	40.597	2.220	2.22098	41	23.8	
116			2.21907		12.6	
206			2.21604		2.1	
611	41.884	2.155	2.15522	14	7.7	
602			2.15768		0.1	
−521	42.099	2.144	2.14493	9	5.2	
031	43.683	2.070	2.07044	17	8.8	
130	43.728	2.068	2.06889	10	2.2	

TABLE I—*Continued*

hkl	2θ	d(obs)	d(calc)	*I*	*I*(cal)	$Cu_6Mo_4O_{15}$(2)
−523			2.06695		7.9	
521	44.004	2.056	2.05628	8	3.7	
−217			2.05179		1.5	
017	44.831	2.019	2.02022	5	2.5	
−516	45.332	1.998	1.99965	5	1.1	
−615	45.656	1.985	1.98448	6	2.3	
−712			1.98717		0.8	
415			1.98796		0.1	
231	45.904	1.975	1.97477	9	2.7	
514		1.975			2.0	
132			1.97881		1.2	
−606	46.843	1.937	1.93778	42	23.5	
620	47.733	1.903	1.90491	7	0.6	
−208			1.90515		2.0	
−233			1.90014		1.0	
−525	48.702	1.868	1.86785	14	6.4	
008			1.86721		9.2	
325			1.87016		5.8	
−802	49.597	1.836	1.83666	11	5.1	
−134			1.83286		2.6	
−624	50.036	1.821	1.82167	17	4.7	
332			1.82064		5.2	
−118			1.82041		0.8	
−318	50.782	1.796	1.79672	21	11.8	
800			1.79852		2.7	
−127	51.039	1.787	1.78824	13	0.1	
134			1.78745		7.1	

[a] Possible MoO_2 impurity.

included in this table are the intensities calculated on the basis of the single crystal results for $Cu_6Mo_5O_{18}$.

Structural determination. Data were collected with an Enraf–Nonius CAD4 X-ray diffractometer equipped with monochromatic Mo$K\alpha$ source using a flat needle of $Cu_6Mo_5O_{18}$ with dimensions (0.09 × 0.17 × 0.45) mm. Twenty-five diffraction maxima were located and used to obtain the cell parameters with dimensions a = 14.676(15), b = 6.280(4), c = 15.254(12) Å, and β = 101.78(3)°. For Z = 4, the calculated density is 5.54 g · cm^{-3}.

A total of 1689 reflections were collected at ambient temperature using the ω scan mode in the range, 4° < 2θ < 50°, with a 1.8–2.0° scan range at 1°/min. There was no evidence of radiation damage to the crystal during data collection. The data were treated in the usual fashion for Lorentz-polarization and absorption (*15*), yielding 1164 independent reflections with $I \geq 3\sigma$. With μ (mm) = 135.06 cm^{-1} and faces defined by (*hkl*, mm): ± [001, 0.045; 011, 0.085; 01$\bar{1}$, 0.095; $\bar{4}$01, 0.238], transmission factors varied from 0.11 to 0.32.

Examination of the data revealed systematic absences compatible with the space group *I*2/*c* (a nonstandard setting of *C*2/*c*, No. 15). The structure was solved using an automated Patterson solution method and refined with anisotropic full-matrix least squares to R = 0.027 and R_w = 0.045, where $R_w = [\Sigma w(|F_o| - |F_c|)^2/\Sigma w|F_o|^2]^{1/2}$ with w proportional to $[\sigma^2(I) + (0.03I)^2]^{-1/2}$. The refinement also included a term for isotropic extinction which resulted in g = 2.64(10) × 10^{-4} mm. The final ESD of an observation of unit weight is 2.79. The largest final difference-Fourier map residual was 0.63 e/Å^3 near Cu(1). The final positional parameters are listed in Table II.[1]

3. Results and Discussion

Based on a comparison of powder patterns (Table I), the earlier reports (*1–6, 10*) of materials of stoichiometry $Cu_6Mo_4O_{15}$ appear to be in error. Prepared in pure form hydrothermally, $Cu_6Mo_5O_{18}$ is shown to melt congruently (Fig. 1). Consequently, it has been possible to prepare single crystals of $Cu_6Mo_5O_{18}$ by direct combination of stoichiometric quantities of the binary oxides. Both ESCA and ESR measurements (*16, 17*) run on freshly prepared samples han-

[1] See NAPS document No. 04338 for 5 pages of supplementary material. Order from ASIS/NAPS, Microfiche Publications, P.O. Box 3513, Grand Central Station, New York, NY 10163. Remit in advance $4.00 for microfiche copy or for photocopy, $7.75 up to 20 pages plus $.30 for each additional page. All orders must be prepaid. Institutions and organizations may order by purchase order. However, there is a billing and handling charge for this service of $15. Foreign orders add $4.50 for postage and handling, for the first 20 pages, and $1.00 for additional 10 pages of material. Remit $1.50 for postage of any microfiche orders.

TABLE II

FRACTIONAL COORDINATES (×10,000) AND ISOTROPIC THERMAL PARAMETERS

Atom	*X*	*Y*	*Z*	B_{iso}
Mo(1)	5000	9320(1)	2500	0.7(1)′
Mo(2)	3389.6(3)	5820.5(8)	2421.9(3)	0.7(1)′
Mo(3)	1586.8(3)	6356.9(7)	711.9(3)	0.7(1)′
Cu(1)	3885.8(6)	6477.8(14)	378.1(6)	1.9(1)′
Cu(2)	2143.6(6)	3799.2(12)	3692.5(6)	1.6(1)′
Cu(3)	5031.0(6)	3043.1(14)	919.8(5)	2.0(1)′
O(1)	4018(3)	3947(7)	3107(3)	1.3(1)′
O(2)	2598(3)	6639(6)	3295(3)	0.8(1)′
O(3)	868(3)	8497(7)	187(3)	1.2(1)′
O(4)	4201(3)	6661(7)	1724(3)	1.1(1)′
O(5)	923(3)	4076(6)	348(3)	1.2(1)′
O(6)	5947(3)	8474(6)	1871(3)	0.9(1)′
O(7)	2452(3)	6328(7)	65(3)	1.2(1)′
O(8)	4346(3)	11043(7)	1700(3)	1.2(1)′
O(9)	2557(3)	4243(6)	1652(3)	1.1(1)′

dled under nitrogen confirm the oxidation state assignments as $Cu_6^{1+}Mo_5^{6+}O_{18}$.

Preliminary 4-probe electrical measurements (*18*) show $Cu_6Mo_5O_{18}$ to be a semiconductor with a room temperature resistivity of $\sim 1.5 \times 10^3$ ohm · cm. The red color of $Cu_6Mo_5O_{18}$ suggests an optical band gap of ~1.9 eV. However, an activation energy of ~0.15 eV, indicative of extrinsic behavior, is determined from the resistivity data. The observation that the resistivity of $Cu_6Mo_5O_{18}$ single crystals decreases irreversibly with gentle heating in an oxygen-containing atmosphere suggests that the creation of Cu^{2+} states is responsible for this extrinsic behavior. Although not quantified, ESR measurements performed at liquid nitrogen temperatures on aged samples clearly indicate the presence of Cu^{2+} states (*17*).

TABLE III

BOND DISTANCES (IN Å) FOR $Cu_6Mo_5O_{18}$[a]: (A) IN STANDARD FORM AND (B) EMPHASIZING THE OXYGEN COORDINATION

a.	Mo(1)–O4	2.235(4)	Mo(2)–O1	1.713(4)	Mo(3)–O2b	2.138(4)
	–O4a	2.235(4)	–O2	2.005(4)	–O3	1.793(4)
	–O6	1.918(4)	–O2b	2.280(4)	–O5	1.757(4)
	–O6a	1.918(4)	–O4	1.829(4)	–O6h	2.167(5)
	–O8	1.761(5)	–O6a	2.112(4)	–O7	1.767(4)
	–O8a	1.761(5)	–O9	1.807(5)	–O9	2.239(5)
	Cu(1)–O3c	2.122(4)	Cu(2)–O2	2.039(4)	Cu(3)–O1a	1.905(5)
	–O4	2.014(5)	–O7	2.051(5)	–O3c	1.939(5)
	–O5d	2.023(4)	–O8	2.148(5)	–O5e	2.171(5)
	–O7	2.063(5)	–O9	2.053(5)	–O8f	2.120(5)
					[–O3k	2.836(5)][b]
					[–O4	2.960(4)]
b.	O1[c]–Mo(2)	1.713	O2–Mo(2)	2.005	O3[c]–Mo(3)	1.793
	–Cu(3a)	1.904	–Mo(2b)	2.280	–Cu(1d)	2.122
			–Mo(3b)	2.138	–Cu(3d)	1.939
			–Cu(2g)	2.039		
	O4–Mo(1)	2.235	O5[c]–Mo(3)	1.757	O6–Mo(1)	1.918
	–Mo(2)	1.829	–Cu(1c)	2.023	–Mo(2a)	2.112
	–Cu(1)	2.014	–Cu(3j)	2.171	–Mo(3k)	2.167
	O7[c]–Mo(3)	1.757	O8[c]–Mo(1)	1.761	O9–Mo(2)	1.807
	–Cu(1)	2.063	–Cu(2d)	2.148	–Mo(3)	2.239
	–Cu(2)	2.051	–Cu(3l)	2.120	–Cu(2c)	2.053

[a] Atom labels refer to Fig. 2.

[b] Long Cu–O bonds associated with the pseudooctahedral coordination of Cu(3).

[c] Molybdenyl oxygens with bond strengths in excess of 1.3 (*33*).

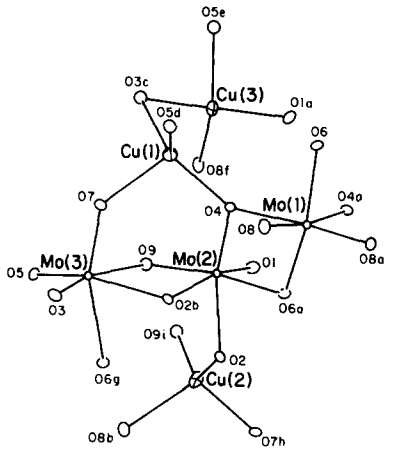

FIG. 2. The metal atoms contained within the asymmetric unit of $Cu_6Mo_5O_{18}$ (shown with full oxygen coordination).

$Cu_6Mo_5O_{18}$ can be described as a three-dimensional structure comprised of Mo–O chains (1-D) and Cu–O layers (2-D). The labeling scheme and oxygen coordination about the independent metal atoms of $Cu_6Mo_5O_{18}$ are illustrated in Fig. 2 (see Tables III and IV for bond distances and coordination geometries). The three independent molybdenum atoms all exhibit octahedral distortions typical of Mo^{6+} oxides (*19*). On the other hand, the tetrahedral coordination of the copper atoms is atypical for Cu^{1+} in an oxide system (*20*). Seven of the nine independent oxygen atoms are three coordinate, while O1 and O2 are two and four coordinate, respectively (Table IIIb). This oxygen coordination results in the formation of a three-dimensional network as illustrated in Fig. 3. Tunnels are readily apparent in this network running along the [100] direction. The unit cell of $Cu_6Mo_5O_{18}$ is shown in Fig. 4.

The structure of $Cu_6Mo_5O_{18}$ is more easily seen as consisting of chains of edge-sharing MoO_6 octahedra and sheets of corner-sharing CuO_4 tetrahedra.

The detailed structure of a single Mo–O chain is shown in Fig. 5a. These chains run parallel to the *a* axis and their stacking is illustrated in Fig. 5b. The Mo–O chains contain three independent edge-sharing MoO_6 octahedra, with each octahedra exhibiting a different type of distortion from octahedral site symmetry (see Tables III and IV). Although a deviation from octahe-

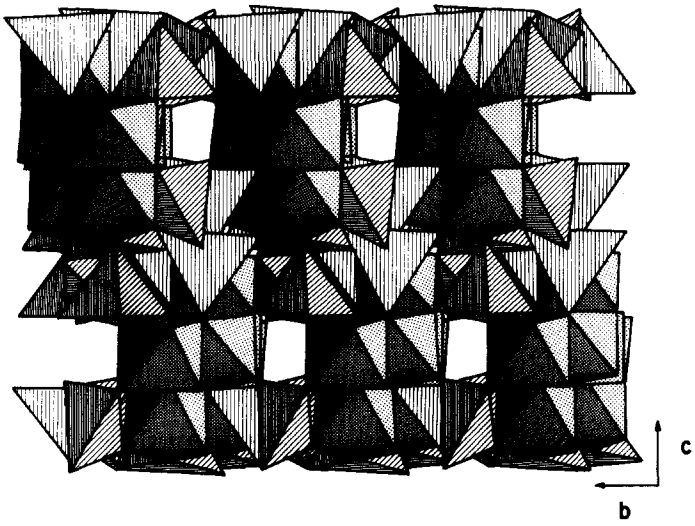

FIG. 3. The structure of $Cu_6Mo_5O_{18}$ revealing tunnels running along [100]. (Polyhedra: Cu, line pattern; Mo, dot pattern).

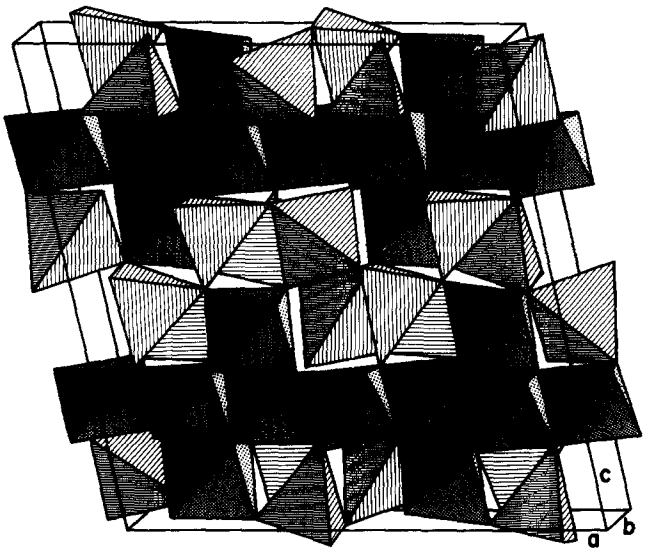

FIG. 4. The unit cell of $Cu_6Mo_5O_{18}$. The polyhedra are completed for clarity. The darker MoO_6 octahedra (dot pattern) are distinguished from the lighter CuO_4 tetrahedra (line pattern).

TABLE IV

COORDINATION GEOMETRIES FOR THE INDEPENDENT ATOMS OF $Cu_6Mo_5O_{18}$

Atom	Polyhedral type	Deviation[a]
Mo(1)	Octahedral	11°
Mo(2)	Octahedral	12°
Mo(3)	Octahedral	11°
Cu(1)	Tetrahedral	8°
Cu(2)	Tetrahedral	7°
Cu(3)	Tetrahedral	16° (octahedral; 10°)[b]
O1	Linear	26°
O2	Tetrahedral	8°
O3	Trigonal	17°
O4	Trigonal	8°
O5	Trigonal	22°
O6	Trigonal	21°
O7	Trigonal	11°
O8	Trigonal	5°
O9	Trigonal	4°

[a] The deviation is equal to the ideal O–M–O angle for a given polyhedron minus the actual average angle observed. (Ideal angles: octa = 90°; tetra = 109.5°; trig = 120°; linear = 180°.)

[b] The coordination about Cu(3) can be considered octahedral with 2 long bonds (*cis*) and 4 short (Table IIIa).

dral site symmetry could be expected for $Cu_6Mo_5O_{18}$ (*21*), it is remarkable to find three types of distortion in a single compound: Mo(1) displays the (2 + 2 + 2) distortion (*22*) typical of MoO_3 itself (*23*); Mo(2) has roughly a (1 + 4 + 1) distortion which is found in $MoO_3 \cdot 2H_2O$ (*24*); and finally, Mo(3) shows a (3 + 3) coordination analogous to that found in a number of *cis*-trioxomolybdenum(VI) complexes (*25, 26*). For all three independent molybdenum atoms, it will be noted that the molybdenyl oxygens (Mo=O; bond lengths to molybdenum <1.8 Å) are coordinated to copper atoms only (see Table IIIb), reflecting the acidic character of these oxygen atoms. The nature of the Mo(VI)–O bonding which leads to these octahedral distortions has been addressed at length by Goodenough (*19*).

The Cu–O sheets stack normal to the *c* axis and a single sheet is detailed in Fig. 6. Within the Cu–O layers, the Cu^{1+} atoms are found to be tetrahedrally coordinated. This is quite unexpected in an oxide system.

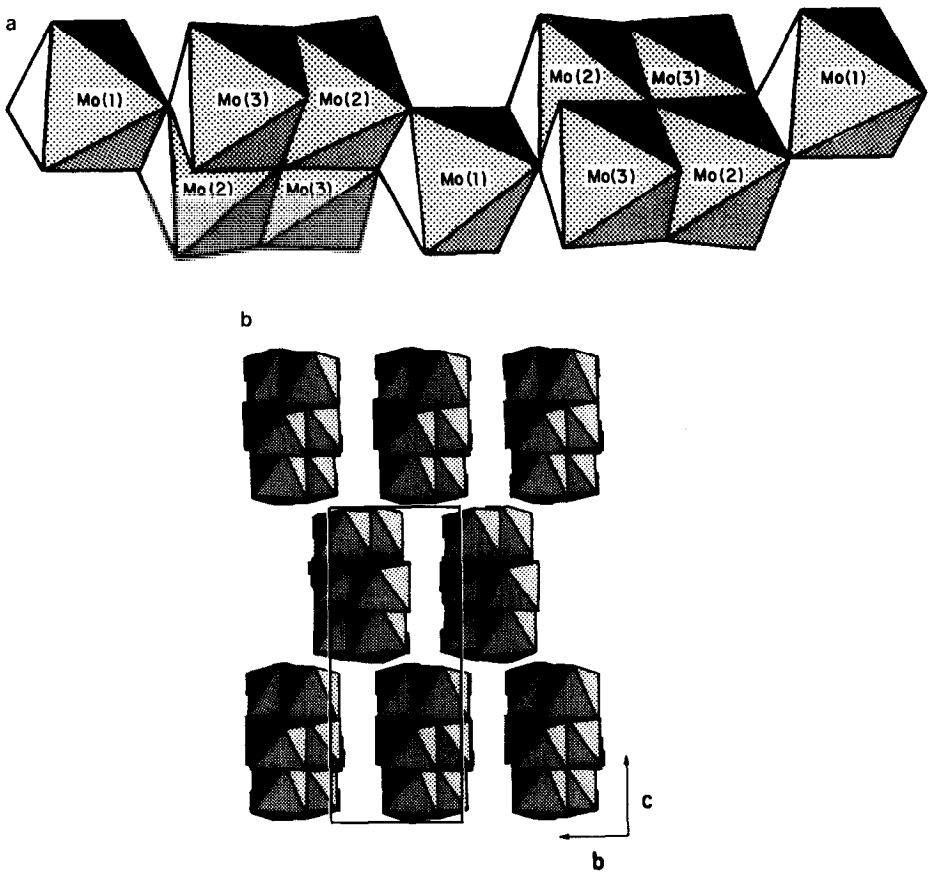

FIG. 5. (a) The repeat unit of the chains of MoO_6 octahedra and (b) the stacking of these chains as viewed down the *a* axis (unit cell outlined).

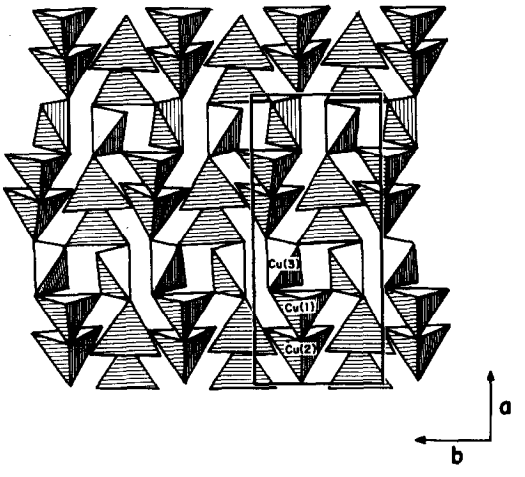

FIG. 6. A sheet of CuO_4 tetrahedra as viewed down the *c* axis (unit cell outlined).

Cu^{1+} is typically found linearly coordinated as in Cu_2O itself (*27*), the Cu^{1+} delafossites (*28*), and a number of alkali metal oxocuprates (*29*). Tetrahedral Cu^{1+} is only found in one other oxide structure, $CuNb_3O_8$ (*30*). In $CuNb_3O_8$ the copper atom sits in a distorted tetrahedron with Cu–O distances ranging from 2.08 to 2.25 Å. Two other adjacent oxygen atoms at 2.43 and 2.49 Å complete a distorted octahedron about the copper. This situation is analogous to that observed for Cu(3) of the present structure (Fig. 7b, Table III). The coordination about Cu(3) is the most highly distorted of the three independent Cu atoms with bond angles close to 90° (see Table IV). In fact the oxygen coordination about Cu(3) appears

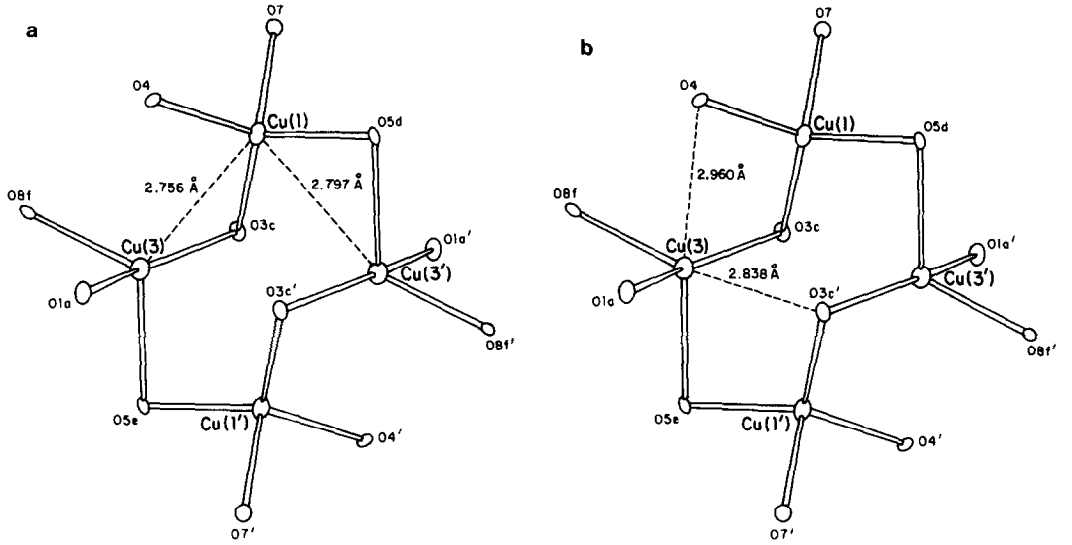

FIG. 7. Details of the coordination of the tetrameric CuO_4 units at the inversion center ($\frac{1}{2}$, $\frac{1}{2}$, 0) (a) emphasizing the short Cu–Cu interatomic distances, and (b) the pseudooctahedral coordination of Cu(3).

pseudooctahedral with long bonds to O(4) and O(3c') (Fig. 7b). In the case of the niobate, substitution of lithium for copper results in the same structure type, only the lithium is found to occupy a more regular octahedral site (*31*). From this observation one would predict that lithium substitution for copper in $Cu_6Mo_5O_{18}$ would take place initially at the pseudooctahedral Cu(3) site. Lithium substitution reactions are currently being investigated.

Another interesting feature of this structure is the existence of tetrameric units of Cu–O tetrahedra formed by Cu(1) and Cu(3) which can be seen in Fig. 6 and are illustrated in Fig. 7. The Cu–Cu distances in this tetrameric unit (Fig. 7a) are only ~0.2 Å longer than the Cu–Cu distance of 2.56 Å found in Cu metal. These short Cu–Cu interactions are of interest as the first example of a so-called Cu^{1+} "aggregate" compound (*32*) observed in an oxide system. Although the preferred d^{10} configuration for Cu^{1+} would argue against metal–metal bonding, the short interaction distances are unusual. For organo-Cu^{1+} aggregate compounds, ligand bridges are found in every case, and it is thought that the short Cu–Cu interactions result from ligand-imposed stereochemical requirements (*32*). For $Cu_6Mo_5O_{18}$, on the other hand, stereochemical arguments do not appear to hold, and one must invoke packing forces if Cu^{1+}–Cu^{1+} bonding is to be avoided.

Finally, on the question of the thermal reduction of $Cu_3Mo_2O_9$, it is evident that there exists no simple "breathing mode" as was postulated previously (*1–7*). Assuming that the thermal reduction results only in the formation of Cu^{1+} and Mo^{6+}, the observation of Nassau and Shiever, namely, that $\frac{3}{4}$ mole of O_2 is produced for every mole of $Cu_3Mo_2O_9$ reduced (from Eq. (2)), leads to

$$Cu_3Mo_2O_9 \rightarrow [Cu_3^{1+}Mo_2^{6+}O_{7.5}] + \tfrac{3}{4}O_2 \quad (6)$$

$$5[Cu_3^{1+}Mo_2^{6+}O_{7.5}] \rightarrow 2Cu_6Mo_5O_{18} + \tfrac{3}{2}Cu_2O. \quad (7)$$

In this work, samples of $Cu_3Mo_2O_9$ thermally reduced at 850°C were subsequently

recrystallized hydrothermally, producing not only $Cu_6Mo_5O_{18}$ but also beautifully faceted, red Cu_2O cyrstals in agreement with Eq. (7). The failure to observe Cu_2O in the previous papers is most likely attributed to the Cu_2O existing as a fine dispersion in the $Cu_6Mo_5O_{18}$ matrix coupled with the complexity of the powder pattern of $Cu_6Mo_5O_{18}$.

Acknowledgments

The authors thank C. Foris for her help in refining the powder pattern data, J. Gillson for making the resistivity measurements, P. Bierstedt for obtaining the ESCA results, and C. Dybowski for providing the ESR results. The authors acknowledge the helpful discussions with Dr. A. W. Sleight.

References

1. K. Nassau and J. W. Shiever, *J. Amer. Ceram. Soc.* **45**(1), 36 (1969).
2. T. Machej and J. Ziolkowski, *J. Solid State Chem.* **31,** 135 (1980).
3. T. Machej and J. Ziolkowski, *J. Solid State Chem.* **31,** 145 (1980).
4. T. Machej and J. Ziolkowski, *Pol. Akad. Nauk.* **30,** 227 (1980).
5. J. Haber and K. Jamroz, *Rev. Chem. Miner.* **20,** 712 (1983).
6. J. Haber, T. Machej, L. Ungier, and J. Ziolkowski, *J. Solid State Chem.* **25,** 207 (1978).
7. I. D. Thomas, A. Herzog, and D. McLachlan, *Acta. Crystallogr.* **9,** 316 (1956).
8. L. Kihlborg, R. Norrestam, and B. Olivecrona, *Acta. Crystallogr. B* **27,** 2066 (1971).
9. L. Katz, A. Kesenally, and L. Kihlborg, *Acta. Crystallogr. B* **27,** 2071 (1971).
10. J. Haber and T. Wiltowski, *Bull. Acad. Pol. Chim.* **29,** 563 (1983).
11. R. A. Laudise (Ed.), "The Growth of Single Crystals," pp. 161–173, Prentice–Hall, Englewood Cliffs, N.J. (1970).
12. Metals were determined by atomic absorption spectroscopy and oxygen was determined by oxygen fusion in an inductively coupled carbon crucible under argon.
13. P. M. de Wolff, *J. Appl. Crystalogr.* **1,** 108 (1968).
14. G. S. Smith and R. L. Snyder, *J. Appl. Crystallogr.* **12,** 60 (1979).
15. P. Coppens, *Acta. Crystallogr.* **18,** 1035 (1965).
16. ESCA spectra were recorded on a DuPont 650 instrument. The spectra were compared with those reported in Ref. (*6*). Freshly prepared $Cu_6Mo_5O_{18}$ samples handled under nitrogen gave a single Cu $2p_{3/2}$ EB line at 932.4 eV, indicative of Cu(I). As the samples aged in oxygen, a second line appeared at 935.2 eV, indicative of Cu(II). For a discussion of the ESCA results, see Ref. (*6*).
17. ESR spectra were recorded on a Bruker ER-420 instrument. The lack of a detectible Cu(II) signal on freshly prepared $Cu_6Mo_5O_{18}$ samples handled under nitrogen implies that copper is present in the 1+ oxidation state. $Cu_6Mo_5O_{18}$ samples aged in oxygen did exhibit a Cu(II) signal at liquid nitrogen temperature. No attempt was made to quantify the amount of Cu(II) present.
18. Detailed measurements of the transport properties of $Cu_6MO_5O_{18}$ are currently under investigation.
19. J. B. Goodenough, "Proceedings of the Climax 4th International Conf. on the Chem. and Uses of Molybdenum" (H. F. Barry and P. C. H. Mitchell, Eds.), pp. 1–22, Climax Molybdenum Co., Ann Arbor, Mich. (1982).
20. A. F. Wells, "Structural Inorganic Chemistry," 4th ed., pp. 879–887, Univ. Oxford Press (Clarendon) (1975).
21. Only in a few instances, such as the ordered perovskites, $A_2^{II}B^{II}MoO_6$, are regular Mo(VI) octahedra observed.
22. The notation refers to the number of *s*hort (molybdenyl, Mo=O) bonds, *i*ntermediate (roughly single) bonds, and *l*ong (fractional) bonds, making up the distorted octahedron: ($s + i + l$). In the case of (3 + 3) there are 3*s* and 3*l*. See also Ref. (*19*).
23. L. Kihlborg, *Arkiv. Chim.* **21,** 357 (1963).
24. B. Krebs, *Acta Crystallogr. B* **28,** 2222 (1972).
25. F. A. Cotton and R. C. Elder, *Inorg. Chem.* **3,** 397 (1964).
26. R. J. Butcher and B. R. Penfold, *J. Cryst. Mol. Struct.* **6,** 13 (1976).
27. M. C. Neuburger, *Z. Krist.* **77,** 169 (1931).
28. (a) C. T. Prewitt, R. D. Shannon, and D. B. Rogers, *Inorg. Chem.* **10,** 719 (1971); (b) T. Ishiguro, N. Ishizawa, N. Mizutani, and M. Kato, *J. Solid State Chem.* **41,** 132 (1982); and *J. Solid State Chem.* **49,** 232 (1983).
29. (a) K. Hestermann and R. Hoppe, *Z. Anorg. Allg. Chem.* **360,** 113 (1968); (b) R. Hoppe, K. Hestermann, and F. Schenk, *Z. Anorg. Allg. Chem.* **365,** 275 (1969); (c) C. L. Teske and H. Müller-Buschbaum, *Z. Naturforsch. B* **27,** 296 (1972); *Z. Anorg. Allg. H-N. Chem.* **379,** 113 (1970); (d) H-N. Migeon, M. Zanne, C. Gleitzer, and A. Courtois, *J. Solid State Chem.* **16,** 325 (1976).
30. B-O. Mardiner, P-E. Werner, E. Wahl-

STRÖM, AND G. MALMROS, *Acta Chem. Scand. A* **34,** 51 (1980).

31. M. LUNDBERG, *Acta Chem. Scand.* **25,** 3337 (1971).

32. For a discussion of Cu^{I}–Cu^{I} interaction see F. A. COTTON AND G. WILKINSON, "Advanced Inorganic Chemistry," 4th Ed., p. 807, Wiley, New York (1980).

33. The bond strength, s, is derived from the expression, $s = (d/1.882)^{-6.0}$ where d is the bond length in Å. Taken from J. C. J. BART AND U. RAGAINI, "Proceedings of the 3rd International Conference on the Chemistry and Uses of Molybdenum" (H. F. Barry and P. C. H. Mitchell, Eds.), Climax Molybdenum Co., Ann Arbor, Mich. (1979).